NUMERICAL EXPERIMENTS ON THE TROPICAL AIR-SEA INTERACTION WAVES

Zhang Renhe (张人禾)

Institute of Atmospheric Physics, Academia Sinica, Beijing 100080

and *Chao Jiping* (巢纪平)

National Research Center for Marine Environmental Forecasts,
State Oceanic Administration, Beijing 100081

Received August 1, 1991

ABSTRACT

By means of the numerical method, the tropical air–sea interaction waves are studied. The results show that when the Kelvin waves are filtered out and only the equatorial Rossby waves are reserved both in the atmosphere and in the ocean, the disturbances can also propagate eastward because of the air–sea interaction. The critical wavelength of the eastward propagating waves is related to the intensity of the air–sea interaction. The stronger the air–sea interaction, the larger the eastward propagating components of the air–sea interaction waves. The results of the numerical experiments are in good agreement with those of the theoretical analysis (Chao and Zhang, 1988).

Key words: equatorial Rossby waves, Kelvin waves, tropical air–sea interaction waves

I. INTRODUCTION

Philander et al. (1984) and Yamagata (1985) have discussed the unstable air–sea interaction in the tropics. Their calculating results showed that the disturbances can propagate eastward because of the air–sea interaction, and they believed that the eastward propagating disturbances were caused by the Kelvin waves after the air–sea interaction. Chao and Zhang (1988) pointed out that there also exist unstable air–sea interaction waves which propagate eastward by means of a simple tropical air–sea coupled model, in which the Kelvin waves are filtered out in both the atmosphere and oceans, and the roles of the tropical air–sea interaction waves in the ENSO events were discussed. In Chao and Zhang' s work, the truncating model method was used in the process of solution, which would undoubtedly affect the results. Here we will solve the tropical air–sea interaction model by using the numerical method instead of the truncating model method, to further study the properties of tropical air–sea interaction waves.

II. NUMERICAL MODEL

1. *Model Equations*

Chao and Zhang (1988) have described the model equations in detail in both the atmosphere and oceans, so we will not reiterate them here. According to Chao and Zhang, the nondimensional equations on the equatorial β–plane in the atmosphere and oceans are given respectively as follows:

$$\left(\frac{\partial^2}{\partial x^2}+\frac{\partial^2}{\partial y^2}-\frac{y^2}{4}\right)\frac{\partial h_a}{\partial t}+\frac{1}{2\varepsilon^{1/2}}\frac{\partial h_a}{\partial x}=\frac{\varepsilon AT}{4}y^2 h_s, \tag{1}$$

$$\left[\varepsilon\left(\frac{\partial^2}{\partial x^2}+\frac{\partial^2}{\partial y^2}\right)-\frac{1}{\varepsilon}\frac{y^2}{4}\right]\frac{\partial h_s}{\partial t}+\frac{\varepsilon^{1/2}}{2}\frac{\partial h_s}{\partial x}=\frac{\gamma T}{D}\left(\frac{\partial^2}{\partial x^2}+\frac{\partial^2}{\partial y^2}\right)h_a, \tag{2}$$

where t, x and y are time, zonal and meridional coordinates respectively; h_a and h_s are disturbed height fields in the atmosphere and oceans respectively; $\varepsilon=C_s/C_a$, $C_s=(g\triangle\overline{T}_z D\alpha)^{1/2}$, $C_a=(gH_a)^{1/2}$, where C_a and C_s are gravity velocities in the atmosphere and oceans respectively; $\triangle\overline{T}_z$, α, D and H_a are the difference of climatological sea temperature between the sea surface and the thermocline, thermal expansion coefficient of sea water, depth of mixed layer and equivalent height in the air, respectively; A and γ are the affecting coefficients of sea to air and air to sea respectively (see Chao and Zhang, 1988); $T=(2\beta C_s)^{-1/2}$, the typical time scale of the motion in the sea. Here we take $\triangle\overline{T}_z=8.0$ K, $D=100$m, $H_a=400$m and $\alpha=3.413\times10^{-4}\mathrm{K}^{-1}$.

2. *The Method of Solution*

Rectangular areas are taken both in the atmosphere and oceans. The nondimensional distance in the zonal direction is taken from −6.45 to 6.45, which corresponds to the dimensional distance from -0.75×10^4km to 0.75×10^4km; while nondimensional distance in the meridional direction is taken from −2.0 to 2.0, which corresponds to the dimensional distance from -2.35×10^3km to 2.35×10^3km. Grid points in the zonal and meridional directions are taken to be 129 and 41 respectively, with the intervals being nondimensional distance 0.1 for both zonal and meridional directions, corresponding to the dimensional distance 117 km, e.g., $\triangle x=\triangle y=d=0.1$. For $\partial h_a/\partial t$, and $\partial h_s/\partial t$, Eqs. (1) and (2) are two elliptic equations, which can be solved by the Gauss–Seidel iterative method with overrelaxation. Setting $Z_a=\partial h_a/\partial t$ and $Z_s=\partial h_s/\partial t$, then we have

$$Z^{k,v+1}_{ai,j}=Z^{k,v}_{ai,j}+\frac{\alpha_a}{\mu_{aj}}\left[Z^{k,v}_{ai+1,j}+Z^{k,v+1}_{ai-1,j}+Z^{k,v}_{ai,j+1}+Z^{k,v+1}_{ai,j-1}-\mu^2_{aj}Z^{k,v}_{ai,j}-F^k_{ai,j}\right], \tag{3}$$

$$Z^{k,v+1}_{si,j}=Z^{k,v}_{si,j}+\frac{\alpha_s}{\mu_{sj}}\left[Z^{k,v}_{si+1,j}+Z^{k,v+1}_{si-1,j}+Z^{k,v}_{si,j+1}+Z^{k,v+1}_{si,j-1}-\mu^2_{sj}Z^{k,v}_{si,j}-F^k_{si,j}\right], \tag{4}$$

$$(i=1,2,\cdots,129;\ j=1,2,\cdots,41)$$

where

$$\mu^2_{aj}=4+\frac{d^2}{4}[(j-21)d]^2,$$

$$\mu^2_{sj}=4+\frac{d^2}{4\varepsilon^2}[(j-21)d]^2,$$

$$F^k_{ai,j}=\frac{\varepsilon ATd^2}{4}[(j-21)d]^2-\frac{d}{4\varepsilon^{1/2}}\left(h^k_{ai+1,j}-h^k_{ai-1,j}\right),$$

$$F^k_{si,j}=\frac{\gamma T}{\varepsilon D}\left(h^k_{ai+1,j}+h^k_{ai-1,j}+h^k_{ai,j+1}+h^k_{ai,j-1}-4h^k_{ai,j}\right)-\frac{d^2}{4\varepsilon^2}\left(h^k_{si+1,j}-h^k_{si-1,j}\right),$$

α_a and α_s are coefficients of overrelaxation. In order to get the fastest convergent rate in the iterative process, according to actual calculating test, the α_a and α_s are taken to be 1.86 and 1.70 respectively. k is the number of time step and v is the time of the iteration.

For the time integration, frog–leap scheme is used, that is,

$$h^{k+1}_{ai,j}=h^{k-1}_{ai,j}+2\triangle t_a Z^k_{ai,j}\ , \tag{5}$$

$$h^{k+1}_{si,j}=h^{k-1}_{si,j}+2\triangle t_s Z^k_{si,j}\ , \tag{6}$$

$$(i=1,2,\cdots,129;j=1,2,\cdots,41)$$

$\triangle t_a$ and $\triangle t_s$ are the time steps of atmospheric equation (1) and oceanic equation (2), respectively. Because the velocity of gravity wave in the atmosphere (C_a) is much larger than that in oceans (C_s), we take $\triangle t_a=0.05$ and $\triangle t_s=0.5$, which correspond to dimensional time 1.6 h and 16 h respectively. During the time integration, we integrate the oceanic equation for one step and then integrate the atmospheric equation for ten steps. This integrating method means that the process of the air–sea interaction is taken approximately as follows: After the heating of the atmosphere by oceans for 16 h, the wind stress of the atmosphere then acts on the ocean. The ocean is integrated for 16 h under the action of this wind stress, then a new heating field is given to the atmosphere by the ocean.

For frog–leap schemes (5) and (6), Matsuno scheme (Matsuno, 1966) is used for the beginning of the numerical calculating, that is,

$$\begin{cases} h^{*2}_{ai,j}=h^1_{ai,j}+\triangle t_a Z^1_{ai,j}, \\ h^2_{ai,j}=h^1_{ai,j}+\triangle t_a Z^{*2}_{ai,j}, \end{cases} \tag{7}$$

$$\begin{cases} h^{*2}_{si,j}=h^1_{si,j}+\triangle t_s Z^1_{si,j}, \\ h^2_{si,j}=h^1_{si,j}+\triangle t_s Z^{*2}_{si,j}, \end{cases} \tag{8}$$

$$(i=1,2,\cdots,129;j=1,2,\cdots,41)$$

where superscripts 1 and 2 are the time steps; $Z^{*2}_{ai,j}$ and $Z^{*2}_{si,j}$ are calculated by $h^{*2}_{ai,j}$ and $h^{*2}_{si,j}$, respectively.

Boundary conditions are taken to be zero, i.e., when $x=\pm$ 6.45 and $y=\pm$ 2.0, set $h_a=h_s=0$. In the grid points, we have

$$\begin{cases} h_{a1,j}=h_{a129,j}=h_{s1,j}=h_{s129,j}=0, \\ h_{ai,1}=h_{ai,41}=h_{si,1}=h_{si,41}=0. \end{cases} \tag{9}$$

$$(i=1,2,\cdots,129;j=1,2,\cdots,41)$$

III. CALCULATING RESULTS

1. *The Basic Solution without the Air–Sea Interaction*

For the purpose of the physical comparison and also for examining the stability of the calculating scheme, first of all, we numerically solve the tropical atmospheric equation (1) and oceanic equation (2) without considering the air–sea interaction. Setting $A=\gamma=0$ in Eqs. (1) and (2), then we have

$$\left(\frac{\partial^2}{\partial x^2}+\frac{\partial^2}{\partial y^2}-\frac{y^2}{4}\right)\frac{\partial h_a}{\partial t}+\frac{1}{2\varepsilon^{1/2}}\frac{\partial h_a}{\partial x}=0, \tag{10}$$

$$\left[\varepsilon\left(\frac{\partial^2}{\partial x^2}+\frac{\partial^2}{\partial y^2}\right)-\frac{1}{\varepsilon}\frac{y^2}{4}\right]\frac{\partial h_s}{\partial t}+\frac{\varepsilon^{1/2}}{2}\frac{\partial h_s}{\partial x}=0. \tag{11}$$

According to the theoretical analysis (Chao and Zhang, 1988), now in the atmosphere and in oceans are the equatorial Rossby waves which propagate westward. At $t=0$, the initial disturbed height field in the atmosphere and oceans are given as below

$$h_s^0=h_a^0=\exp[-2(x^2+y^2)]. \tag{12}$$

Fig. 1 shows the evolutions of the disturbed height fields h_a and h_s in the atmosphere

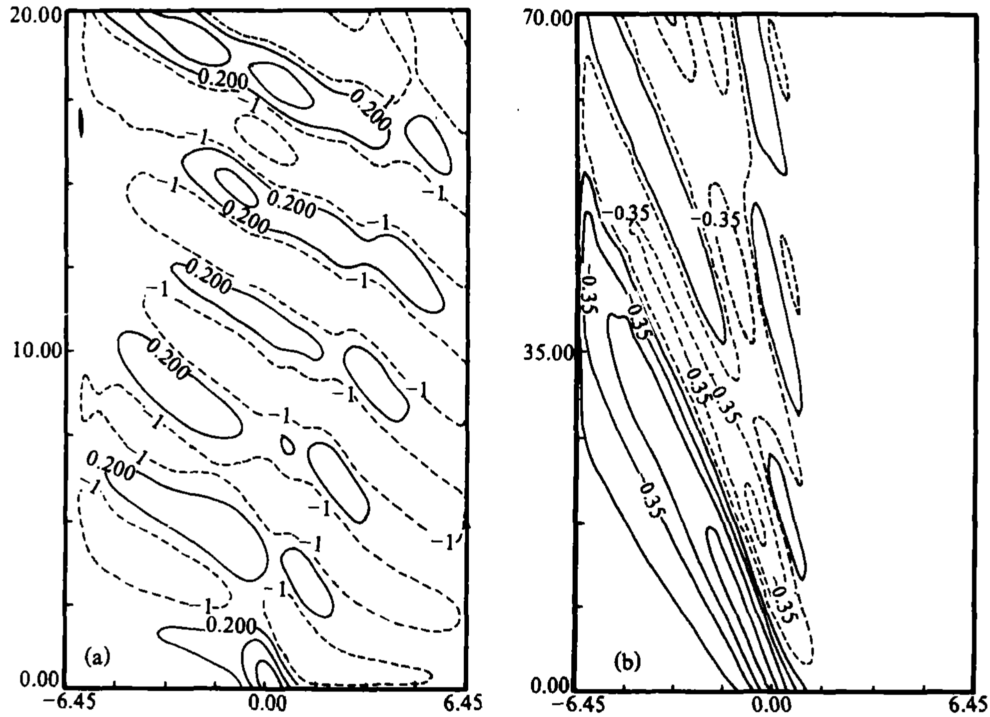

Fig. 1. The evolution of the disturbed height field in the atmosphere (a) and that in the ocean (b) along the equator (the ordinate denoting nondimensional time with 1 corresponding to 32 h, solid lines and dotted lines standing for positive and negative disturbed height respectively).

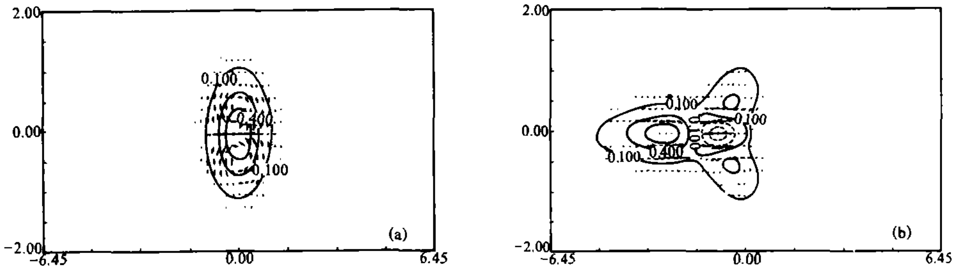

Fig. 2. The initial disturbed field (a) and the disturbed field at 26.7 d (b) in the sea (solid and dotted lines being the same as in Fig. 1, arrows representing the ocean current field).

and oceans along the equator. Because only the equatorial Rossby waves can be found in both the media, then the disturbed height fields are all moving westward. The westward propagating velocity of the disturbed height field in the air is about −18.7 m / s and that in the sea is about −1.3 m / s, which is much smaller than that in the air. The oscillation of the disturbed height field in the air is of high frequency with the period about 4.5 d, while that in the sea is of slowly changing, with the period about 48 d. Fig. 2 shows the initial and the 26.7 th day disturbed fields in the sea. We can see that the disturbed field goes westward and at 26.7 d, the structure of disturbed field is much different from the initial field.

2. *Solutions to General Cases*

At the initial time, we take the initial field of Eq. (12) at $t=0$ in the sea (see Fig. 2a), that is, there only exists the initial disturbed field in the sea, while nothing exists in the air, which means that at this time the sea gives a heating field to the air (see Chao and Zhang, 1988). With $A=10^{-2}\text{s}^{-1}$ and $\gamma=5.0\times 10^{-5}\text{m/s}$. Fig.3 shows the disturbed fields in the atmosphere and oceans respectively at time 26.7 d. Compared with the case without the air–sea interaction (see Fig. 2b), it can be seen that there are great changes in the structure of disturbed field between two cases. When the air–sea interaction is cut off, in the ocean the disturbed field near the equator has a positive disturbed height area in the western part and a negative one in the eastern part, while to the higher latitudes both in the north and south directions of the negative disturbed height area there exists a positive disturbed height area respectively; When the air–sea interaction is taken into account, in the ocean the phase of the disturbed height field in the west–east direction near the equator is just opposite to that without the air–sea interaction. Namely, there is a positive disturbed height area in the eastern part and a negative one in the western part, while the positive disturbed height areas to the south and north of the negative disturbed height area in the higher latitudes disappear. These indicate that the structure of equatorial Rossby waves in the ocean is changed by the air–sea interaction.

Fig.4 shows the evolution of the disturbed height fields in the atmosphere and oceans along the equator. It can be seen that either in the atmosphere or in the ocean there exist two kinds of disturbances, one is of high frequency and the other is of low frequency. For the low–frequency disturbances, they go westward with a velocity about −0.73 m / s, which is smaller than that in the ocean without the air–sea interaction. From Figs. 3 and 4, we can also see that the low–frequency disturbances in the atmosphere and oceans are mainly negatively correlated. Fig.4

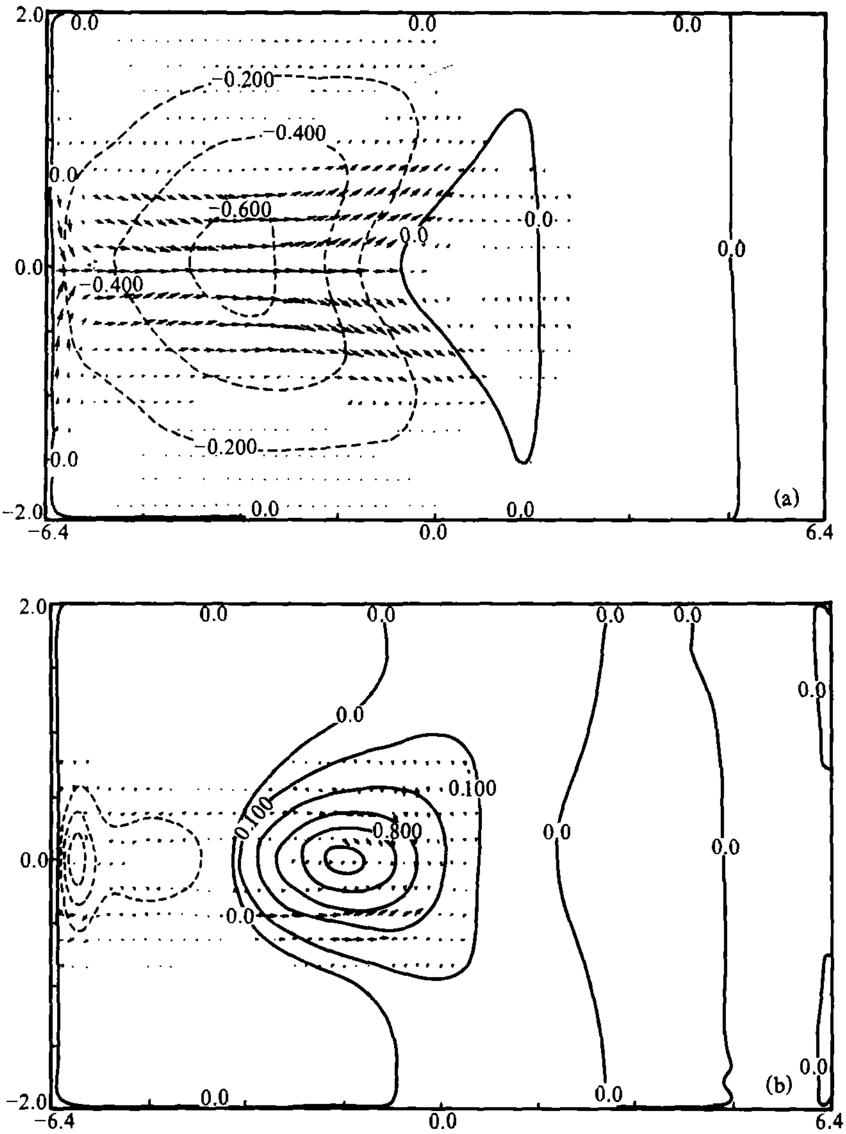

Fig. 3. The disturbed fields in the atmosphere (a) and oceans (b) at time 26.7 d (explanations as Fig. 2, but the arrows in the upper part standing for the wind field).

indicates that the amplitudes of the low–frequency disturbances in both the atmosphere and oceans decay with time, which is in good agreement with the results of the theoretical analysis (Chao and Zhang, 1988).

Fig. 4 also shows that for the high–frequency disturbance in the tropical air–sea coupled system, the period is about 4.5 d, which is very close to that in the atmosphere without the air–sea interaction. From the evolution of the disturbed height field in the atmosphere along the equator (Fig. 4a), we can see that the high–frequency disturbances propagate westward. In the theoretical analysis (Chao and Zhang, 1988), we have already known that the high–

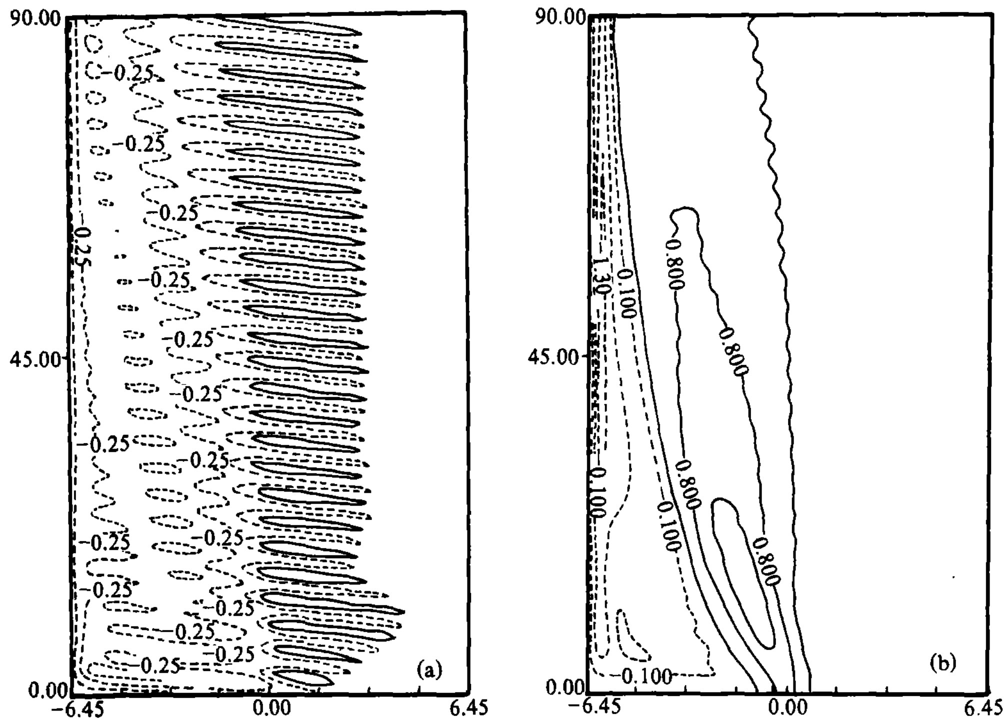

Fig. 4. The evolution of the disturbed height fields in the atmosphere (a) and that in the ocean (b) along the equator (explanations as Fig.1).

frequency tropical air–sea interaction waves are very close to the equatorial Rossby waves in the atmosphere, which is also proved by the numerical calculating results here.

Fig. 5 shows the evolution of the disturbed height fields in the atmosphere and oceans along the equator when the air–sea interaction is intensified. Setting $A\gamma = 2.0 \times 10^{-6}$m / s, from Fig. 5a we can see that the westward propagating component of the low–frequency disturbances reduces, while the eastward propagating component of the low–frequency disturbances enlarges. When the air–sea interaction is further intensified, e. g., setting $A\gamma = 4.5 \times 10^{-6}$m / s, Fig.5b shows that the westward propagating component of the low–frequency disturbances disappears. Now all the low–frequency disturbances both in the atmosphere and in the ocean move eastward. Here we can see that the stronger the air–sea interaction, the larger the eastward propagating component of the low–frequency disturbances in the air–sea coupled system. Fig. 5 also indicates that when the air–sea interaction is intensified, the low–frequency disturbances propagate eastward in the form of a wave train. In the process of propagating, the disturbances in the eastern part is decaying, while those in the western part is intensifying. Thus we can suppose that although the phase speed of the low–frequency disturbances is propagating eastward, the energy is dispersing westward. In addition, Fig. 5 shows that the intensification of the air–sea interaction has little effects on the high–frequency disturbances. Their periods are also about 4.5 d and from the evolution of the disturbed height field in the atmosphere along the equator, we can see that the high–frequency disturbances also propagate westward.

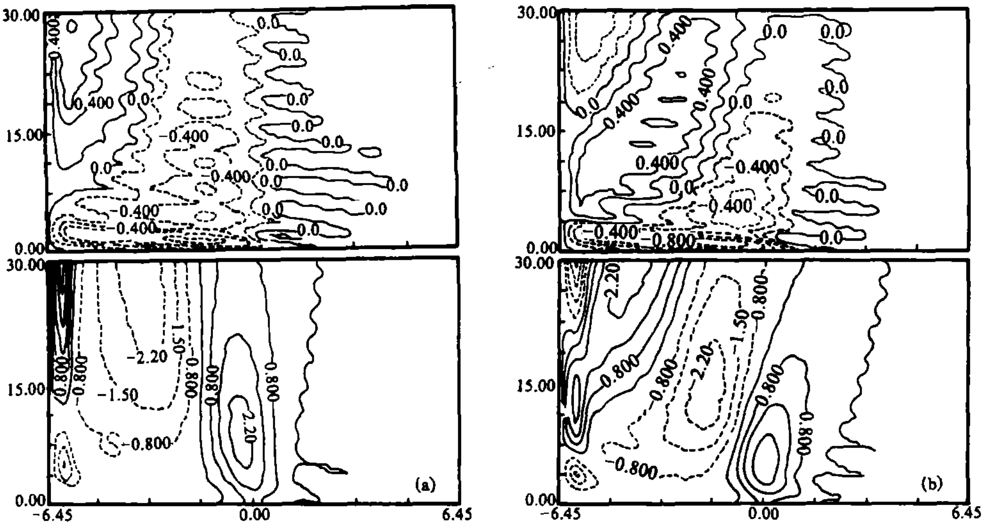

Fig. 5. The evolution of the disturbed height fields in the atmosphere (upper part) and that in the ocean (lower part) along the equator. (a) and (b) correspond to $A\gamma = 2.0 \times 10^{-6}$m / s and 4.5×10^{-6}m / s, respectively (explanations as Fig. 1).

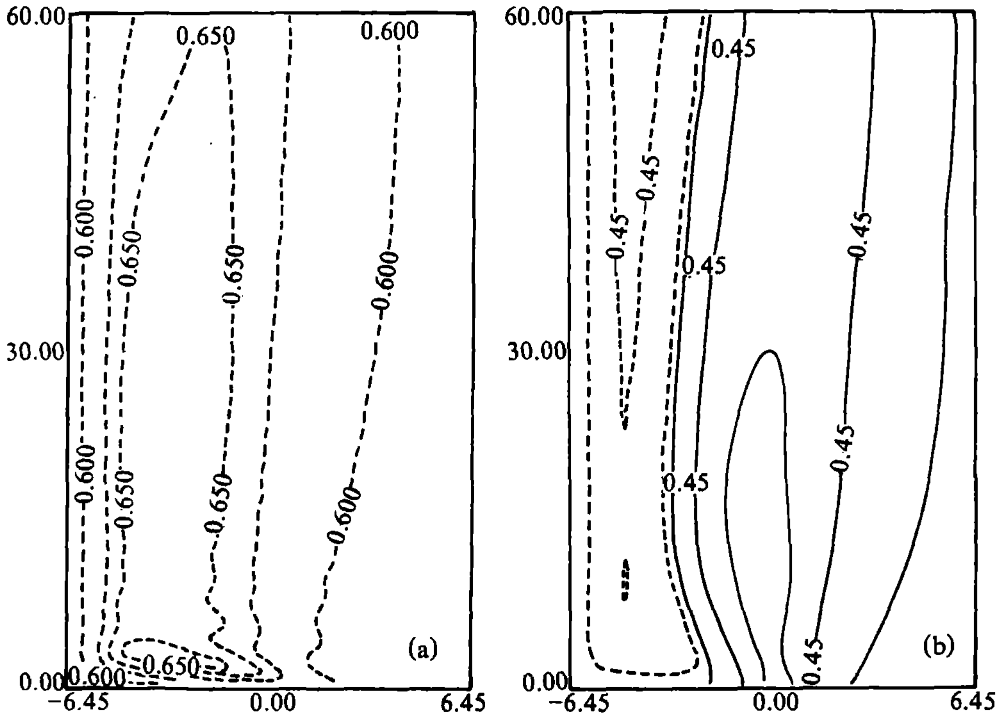

Fig. 6. As in Fig. 4, except that the initial field $h_s^{'0}$ is taken.

3. *Effect of the Initial Fields on the Tropical Air–Sea Interaction Waves*

According to Chao and Zhang (1988), the eastward propagating waves appear in the scope of comparatively long wavelengths. In order to prove this, set $A\gamma = 0.5 \times 10^{-6}$m / s and take the initial field as follows

$$h_s'^0 = \exp[-0.4x^2 - 2y^2]. \tag{13}$$

Compared with Eq. (12), Eq. (13) is equivalent to enlarging the scope of the initial field in the zonal direction. $h_s'^0$ in Eq. (13) and h_s^0 in Eq. (12) correspond to e–fold scales in zonal direction about 1850 km and about 827 km, respectively, i.e., the initial field (13) gives prominence to the effect of the long wave components in fact. In order to reduce the effect of the short wave components, we enlarge the intervals between the grid points in the zonal direction by taking $\triangle x = 0.5$, corresponding to dimensional distance about 585 km.

Fig. 6 shows that when the initial field (13) is used, the evolution of the disturbed height fields in the atmosphere and oceans along the equator. We can see that the disturbed height fields in both the atmosphere and oceans move toward eastward simultaneously. Thus, we know that if the initial field is composed of the waves with comparatively long wavelengths, the westward propagating disturbances (see Fig. 4) can become eastward propagating. From the above

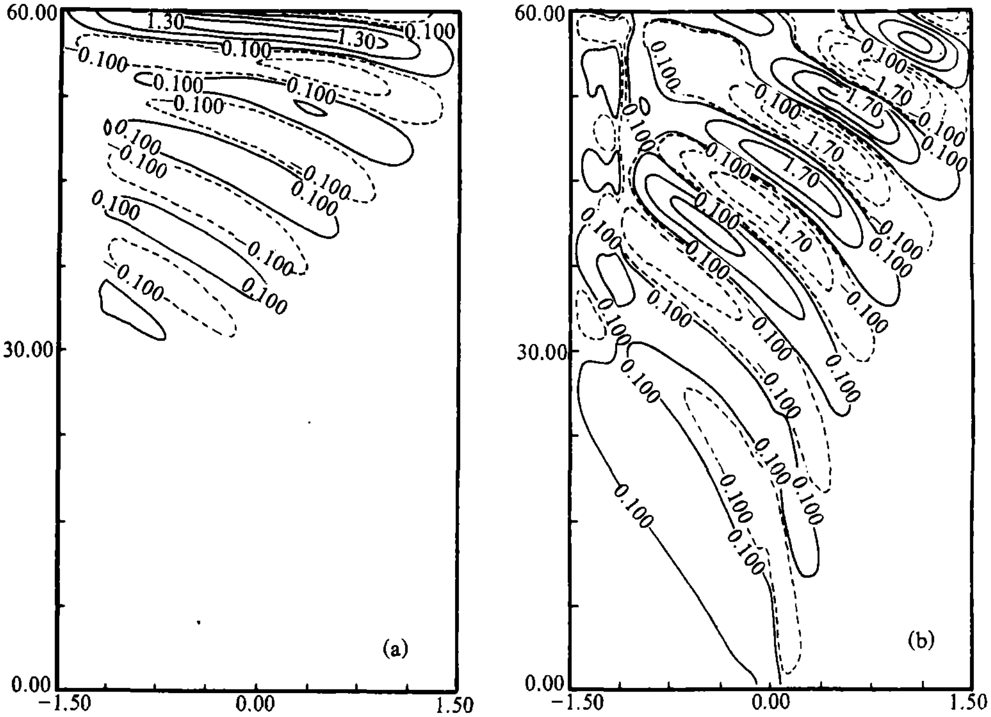

Fig. 7. As in Fig. 4, except that the initial field $h_s''^0$ is taken.

we can see that the eastward propagating waves mainly appear in the scope of comparatively long wavelengths, which is consistent with the results of the theoretical analysis (Chao and Zhang, 1988).

We have known the situation when the initial field is composed of the waves with comparatively long wavelenghts. In the following, we will discuss the situation when the initial field is composed of the waves with comparatively short wavelengths. Setting the initial field as

$$h_s^{''0} = \exp(-200x^2 - 2y^2), \tag{14}$$

it can be seen that Eq. (14) has much less scope in the zonal direction than that of Eq. (12). The e–fold scale that $h_s^{''0}$ corresponds to is about 83 km. In order to take more short wave components into account, in calculating we reduce the intervals between the grid points in the zonal direction by taking $\triangle x = 0.01$, corresponding to the dimensional distance about 11.7 km.

Fig. 7 shows that when the initial field $h_s^{''0}$ is taken, the evolution of the disturbed height fields in the atmosphere and oceans along the equator. From Fig. 7 we can see that although the phase speed of the disturbed height fields propagate westward, the energy of the disturbances disperses eastward. During the process of the eastward dispersing of the energy, the amplitudes of the disturbances are unstably amplified with the increasing of the time, meaning that the energy of the short wave component in the tropical air–sea interaction waves has the characteristics of unstably eastward dispersing.

IV. CONCLUSIONS

According to the analysis above, we can see that when the equatorial Rossby waves in the atmosphere and oceans are coupled together, the coupled waves have the eastward propagating components, which are different from the eastward propagating Kelvin waves. The structure of the tropical air–sea interaction waves is different from that of the equatorial Rossby waves. The propagating direction of the tropical air–sea interaction waves is governed by the intensity of the air–sea interaction. In the general case, the tropical air–sea interaction waves propagate westward. But when the air–sea interaction is intensified, the propagating direction of the tropical air–sea interaction waves can become eastward, and the eastward propagating air–sea interaction waves mainly appear in the scope of comparatively long wavelengths. For the eastward propagating tropical air–sea interaction waves, though the phase speed is eastward, the energy disperses westward. And for the short wave components of the tropical air–sea interaction waves, the phase speed is westward, while the energy unstably disperses eastward.

The results of the numerical experiments also indicate that the air–sea interaction has little effects on the propagating direction and the period of the high–frequency tropical air–sea interaction waves, which are always very close to the equatorial Rossby waves in the atmosphere. Thus we can see that in the long period process of the tropical air–sea coupled system, the equatorial Rossby waves in the ocean play a very important part.

For the convenience of theoretical analysis, truncating model method was used by Chao and Zhang (1988). By using the numerical method to solve Eqs. (1) and (2) directly, the same results as Chao and Zhang (1988) are obtained, which further demonstrate the importance of the air–sea interaction waves in the tropical air–sea coupled system.

REFERENCES

Chao Jiping and Zhang Renhe (1988), The air–sea interaction waves in the tropics and their instabilities, *Acta Meteorologica Sinica*, **2**: 275—287.

Matsuno, T. (1966), Numerical integration of the primitive equations by a simulated backward difference method, *J. Meteor. Soc. Japan*, **44**: 76—84.

Philander, S. G. H., Yamagata, T. and Pacanowski, R. C. (1984), Unstable air–sea interaction in the tropics, *J. Atmos. Sci.*, **41**: 604—613.

Yamagata, T. (1985), Stability of a simple air–sea coupled model in the tropics, *Coupled Ocean–Atmosphere Model*, ed. J. C. J. Nihoul, Amsterdam, 767pp.